Modification of Nanocrystalline WO 3 with a Dicationic Perylene Bisimide: Applications to Molecular Level Solar Water Splitting

ARTICLE *in* JOURNAL OF THE AMERICAN CHEMICAL SOCIETY · APRIL 2015

Impact Factor: 12.11 · DOI: 10.1021/jacs.5b01519 · Source: PubMed

8 AUTHORS, INCLUDING:

Zois Syrgiannis
ITM-CNR, Padua, Italy
33 PUBLICATIONS **198** CITATIONS
SEE PROFILE

Stefano Caramori
University of Ferrara
49 PUBLICATIONS **1,515** CITATIONS
SEE PROFILE

Vito Cristino
University of Ferrara
14 PUBLICATIONS **261** CITATIONS
SEE PROFILE

Carlo Alberto Bignozzi
University of Ferrara
203 PUBLICATIONS **8,649** CITATIONS
SEE PROFILE

JACS
JOURNAL OF THE AMERICAN CHEMICAL SOCIETY
Communication
pubs.acs.org/JACS

Modification of Nanocrystalline WO_3 with a Dicationic Perylene Bisimide: Applications to Molecular Level Solar Water Splitting

Federico Ronconi,[†] Zois Syrgiannis,[§] Aurelio Bonasera,[§] Maurizio Prato,*[,§] Roberto Argazzi,[‡] Stefano Caramori,*[,†] Vito Cristino,[‡] and Carlo Alberto Bignozzi*[,†]

[†]Department of Chemistry and Pharmaceutical Sciences and [‡]CNR-ISOF c/o Department of Chemistry and Pharmaceutical Sciences, University of Ferrara, Via Fossato di Mortara 17, 44121 Ferrara, Italy

[§]Department of Chemical and Pharmaceutical Sciences, University of Trieste, Piazzale Europa 1, 34127 Trieste, Italy

Supporting Information

ABSTRACT: [(*N*,*N*′-Bis(2-(trimethylammonium)-ethylene) perylene 3,4,9,10-tetracarboxylic acid bisimide)-$(PF_6)_2$] (**1**) was observed to spontaneously adsorb on nanocrystalline WO_3 surfaces via aggregation/hydrophobic forces. Under visible irradiation (λ > 435 nm), the excited state of **1** underwent oxidative quenching by electron injection (k_{inj} > 10^8 s^{-1}) to WO_3, leaving a strongly positive hole (E_{ox} ≈ 1.7 V vs SCE), which allows to drive demanding photo-oxidation reactions in photoelectrochemical cells (PECs). The casting of IrO_2 nanoparticles (NPs), acting as water oxidation catalysts (WOCs) on the sensitized electrodes, led to a 4-fold enhancement in photoanodic current, consistent with hole transfer from oxidized dye to IrO_2 occurring on the microsecond time scale. Once the interaction of the sensitizer with suitable WOCs is optimized, **1**/WO_3 photoanodes may hold potentialities for the straightforward building of molecular level devices for solar fuel production.

By the term artificial photosynthesis[1] one generally indicates the possibility of harvesting and converting, by molecular means, solar energy into chemical energy stored in fuels. One of the most attractive artificial photosynthetic conversion schemes involves water splitting in oxygen and hydrogen, which would lead to a virtually inexhaustible source of carbon free energy. Hydrogen is also a valuable chemical by itself, being used as a reactant in a variety of chemical processes including CO_2 reduction.

Artificial photosynthesis requires the interlacing of several molecular components having different roles (light harvesters/antennae/charge separators/catalysts), which act in a concerted way, to overcome energy wasting processes[2] (i.e., deactivation of the excited state and recombination of the charge separated states) that are difficult to avoid with molecular species in homogeneous phase. The interfacing of the photoactive molecular assembly with a conductive or semiconductive solid[3] appears to be an interesting way to control some of the recombination processes, for example, by separating and confining electrons and holes into different phases,[4] or by exploiting the electric fields in the solid (space charge) or at the solid/solution interface to direct the charge carriers in the desired direction.

The four electron oxidation of water is the most demanding part of the water splitting reaction, under both thermodynamic ($E°$ = 1.23 V vs NHE) and kinetic aspects,[5] and most efforts have been concentrated in devising efficient methods to drive this anodic reaction. Water splitting using the powerful oxidizing holes of stable high band gap semiconductors (SCs), mostly metal oxides or oxy-nitrides, including TiO_2,[6] WO_3,[7] Fe_2O_3,[8] and TaON,[9] is relatively well established, although the theoretical efficiencies expected by these materials are often far from being achieved. However, the exploitation of molecular level sensitized photoelectrodes in water splitting reactions, requiring careful dye and surface engineering,[10] is generally less successful due to the lack of stability of the molecular assemblies on the SC surface and to efficient charge recombination processes. The main problem in the molecular approach is the development of visible absorbing sensitizers, having sufficient driving force to carry out both charge injection into the semiconductor and hole transfer to a catalyst, achieving the primary charge separated state. The catalyst should be able to promote, either in a stepwise or concerted way, water oxidation without recombining with electrons injected in the SC, according to the following general reaction scheme:

$$S + h\nu \rightarrow S^* \quad \text{(photoexcitation)} \tag{1}$$

$$S^* \rightarrow S^+ + e_{CB}^- \quad \text{(electron injection)} \tag{2}$$

$$S^+ + C \rightarrow S + C^+ \quad \text{(electron transfer)} \tag{3}$$

$$4C^+ + 2H_2O \rightarrow 4C + 4H^+ + O_2 \quad \text{(hole transfer)} \tag{4}$$

where S is the sensitizer, C is the catalyst, and CB is the SC conduction band.

Recently Finke et al.[11] focused the attention on the assembly of a modified perylene bisimide (PBI) dye onto ITO electrodes in combination with Co-pi.[12] In this configuration the main limitation, to achieve efficient photoelectrochemical water splitting, is the low light harvesting of the nonporous electrodes.

Perylenes are simple organic molecules possessing high molar extinction coefficient and good thermal and photochemical stability.[13] Most importantly, they show high oxidation potentials, resulting compatible with the activation of many WOCs reported in literature, including ruthenium,[14] iridium,[15] nickel,[16] and iron[17] based catalysts, but are limited by a low

Received: February 11, 2015

DOI: 10.1021/jacs.5b01519
J. Am. Chem. Soc. XXXX, XXX, XXX−XXX

excited state oxidation potential. This fact precludes charge injection into many SCs and, in general, their use in energy conversion schemes relying on the oxidative quenching of their excited state.

Herein we report on the sensitization of nanocrystalline WO_3 with the dicationic dye **1** (**1** = [(*N*,*N*′-bis(2-(trimethylammonium)ethylene) perylene 3,4,9,10-tetracarboxylic acid bisimide) $(PF_6)_2$]), reported in Figure 1, which was demonstrated capable to transfer photogenerated holes to sacrificial species in solution and to codeposited IrO_2 nanoparticles (NPs) acting as WOCs.

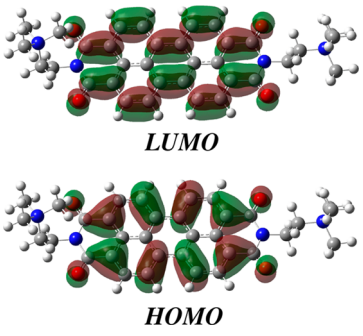

Figure 1. Optimized geometries and frontier molecular orbitals of **1** used in SC sensitization, computed at DFT level in acetonitrile (ACN).

Compound **1** is characterized by a planar geometry of the aromatic core, while the ethyl-trimethylammonium chains are bent over the π-plane with a dihedral angle close to 90°. The HOMO−LUMO energy gap of 2.48 eV is in good agreement with both the electrochemical gap (2.5 eV; E_{ox} = 1.7 V vs SCE; E_{red} = −0.8 V vs SCE, Figure S1) and with the spectroscopic energy gap of 2.36 eV evaluated in ACN solution (Figure S2). The resulting excited state oxidation potential (E_{ox}*) is −0.66 V vs SCE.

Despite the lack of specific anchoring groups, **1** was shown to functionalize porous SCs, including ZrO_2, TiO_2, SnO_2, and WO_3, probably due to aggregation/hydrophobic interactions demonstrated by the blue shift and by a substantial modification of the vibrational structure of the absorption spectrum on the surface, consistent with the probable formation of H aggregates.[18] Similar spectral features, summarized by a main band in the 470−500 nm interval and by a shoulder at ca. 550 nm, are present with slight variations in all sensitized surfaces considered by this study (Figure S3A). Thin WO_3 films (~700 nm) reach a maximum optical density of ca. 0.25 at ~470 nm. On other SC substrates the maximum absorbance was intentionally kept at comparable values. Upon illumination (AM 1.5 G + 435 nm cutoff filter) of the resulting photoanodes in the presence of sacrificial electron donors, including ACN/0.1 M LiI (Figure 2) and aqueous 0.1 M ascorbic acid at pH 3 (Figure S4), a photoanodic current was observed, consistent with charge injection from PBI^{2+} to WO_3 and hole transfer to the sacrificial hole scavenger. The photoanodic current, reaching maximum values of ca. 0.5 mA/cm^2 in the case of WO_3 at a bias of 0.35 V vs SCE, varies in the order WO_3 > SnO_2 > TiO_2. The same trend and similar photocurrent densities are found in ascorbic acid, where, however, TiO_2 was not considered due to the formation of $Ti^{(IV)}$ ascorbates acting as sensitizers.[19]

The poor performance observed with TiO_2 was attributed to the inefficient injection by the excited state of **1**, having insufficient driving force for competing with its photophysical

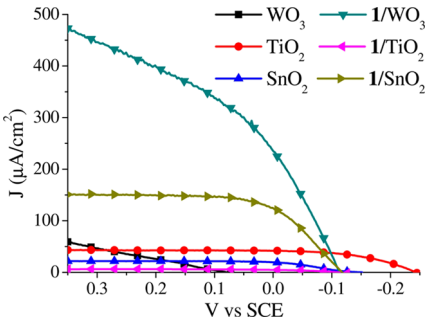

Figure 2. *J*−*V* curves of the **1** sensitized electrodes in the presence of ACN/0.1 M LiI. The photocurrent density (*J*) of each electrode was obtained by subtraction of the respective dark current.

deactivation pathways. Indeed, the study of the emission lifetimes of **1** loaded on SC substrates (TiO_2, SnO_2 and WO_3) compared to inert ZrO_2 thin films, where charge transfer is thermodynamically forbidden, reveals that quenching increases in the order WO_3 > TiO_2 > SnO_2 > ZrO_2, providing a lower estimate to the injection rate constant[20] $k_{inj}(WO_3)$ of 0.4×10^9 s^{-1}, which is 4 to 8 times larger than that found for SnO_2 ($k_{inj}(SnO_2) = 0.1 \times 10^9$ s^{-1}) and TiO_2 ($k_{inj}(TiO_2) = 0.05 \times 10^9$ s^{-1}), respectively (Figures S5−S10 and Table S1).

Additional photoelectrochemical measurements, carried out with optimized WO_3 (SC6) and SnO_2 (SC2) spin coated electrodes (Figure S11 and Supporting Information (SI) section 2.5) in ACN/0.1 M LiI, confirmed a superior performance of WO_3 in generating higher photocurrent (~2.2 mA/cm^2) and, more significantly, superior fill factor (28% vs 23%) and photovoltage ($V_{OC}(WO_3) = -100$ mV vs SCE; $V_{OC}(SnO_2) = -50$ mV vs SCE) (Figure S12). All these figures are consistent with a more effective charge separation on the WO_3 substrate with respect to SnO_2.

Transient absorption measurements, in the ns/μs time scale, agree with the observation of a faster and more efficient formation of the charge separated state ($\mathbf{1}^+/e^-$(CB)) on WO_3. The photophysical behavior of **1** in solution, upon 532 nm nanosecond laser excitation, is dominated by the decay of the lowest singlet excited state, resulting in the bleaching of the ground state and in the appearance of the strong stimulated emission with a clear vibronic progression starting from 530 nm (Figure S13). Similar characteristics are found on ZrO_2 (Figure S14), where the longer lived ground state bleaching suggests population of the triplet state via spin−orbit coupling (SOC) induced by heavy atom (Zr) effect in the proximities of the chromophore.

By contrast on WO_3 (Figure 3) the magnitude of the residual emission of **1** is greatly reduced with respect to the ground state bleaching, and most importantly, the rise of a characteristic absorption in the blue region of the visible spectrum, between 400 and 450 nm, with maximum at ca. 430 nm can be observed, reaching the maximum intensity within 100 ns after excitation. At 300 ns after the laser pulse a significant absorption is still evident, while the ground state bleaching at 470 nm undergoes a significant recovery. The transient absorption in the blue region was thus assigned to the formation of the photo-oxidized dye resulting from charge injection into WO_3. The electron recapture by the oxidized perylene derivative, occurring in the microsecond time scale, is at least 10^3 slower than injection, indicating a favorable kinetic competition for obtaining and storing a primary long-lived charge separated state ($\mathbf{1}^+/e^-(WO_3)$), which may constitute the basis for solar fuel production in a PEC. On SnO_2

DOI: 10.1021/jacs.5b01519
J. Am. Chem. Soc. XXXX, XXX, XXX−XXX

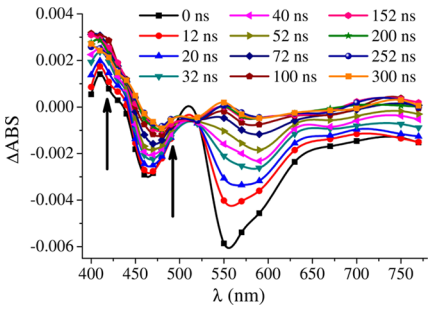

Figure 3. Transient absorption spectra of **1** loaded on WO_3 thin film in the presence of aqueous 0.1 M $NaClO_4$ at pH 3, with 532 nm laser excitation (fwhm 7 ns) and oscilloscope input resistance of 350 Ω.

electrodes (Figure S15), the signature of the charge separated state is much less evident, consistent with the slower charge injection observed in emission quenching experiments.

The ability to exploit relatively energetic photogenerated holes, located on surface adsorbed **1** in artificial photosynthetic processes, was tested in the presence of codeposited IrO_2 NPs, prepared according to the directions of Mallouk et al.[21] Herein IrO_2 was chosen for convenience as an example of catalyst known for having stability and good activity[22] toward water oxidation in acidic media. Different codeposition methods of IrO_2 NPs on sensitized WO_3 films were explored (SI section 2.7). The different photoanodes, named type ***a*–*e*** after the IrO_2 modification route, are briefly summarized in Tables 1 and S2.

Table 1. Types of 1/WO_3 photoanodes modified with IrO_2

electrode	deposition method of IrO_2 NPs on **1**/WO_3
a	without IrO_2 NPs
b	drop casting
c	spin coating
d	spin coating and drying with warm air
e	soaking

Under AM 1.5 G illumination, with 435 nm cutoff filter, without sacrificial agents in aqueous 0.1 M $NaClO_4$ at pH 3, all IrO_2 codeposited electrodes exhibit a photoanodic behavior with photocurrent at 0.5 V vs SCE decreasing in the order ***d*** > ***e*** > ***c*** > ***b*** > ***a***, reaching maximum values close to 70 $\mu A/cm^2$, with a good reproducibility, testified by the small amplitude of the error bars (Figure 4A), obtained for batches of three identical electrodes.

The lowest photocurrent onset, observed at ca. 0.3 V vs SCE, is obtained with type ***c*** and ***d*** electrodes (spin coated IrO_2), which also produce a higher photocurrent density at voltages ranging from 0.28 to 0.43 V vs SCE. It is clear that the presence of IrO_2 allows for a ∼6-fold enhancement of the photoanodic current density compared to the simple type ***a*** electrodes (**1**/WO_3) consistent with hole transfer from photogenerated $\mathbf{1}^+$ to IrO_2, which in turn catalyzes water oxidation. IPCE (Figure 4B) undergoes a doubling when moving from type ***a*** to type ***c*** electrodes, with a photocurrent response in good agreement with the absorption spectrum of the sensitizer. The corresponding APCE values thus increase from ca. 0.5% to ca. 1% in the IrO_2 treated photoanode (Figure S16).

The *J*–*V* curves collected under shuttered illumination (Figure 4C) reveal photocurrent transients reaching ∼200 $\mu A/cm^2$, at a potential close to 0.5 V vs SCE (type ***c*** and ***d*** electrodes), which are clearly larger than the photoanodic current collected under steady state conditions (Figure 4A). The overshooting of

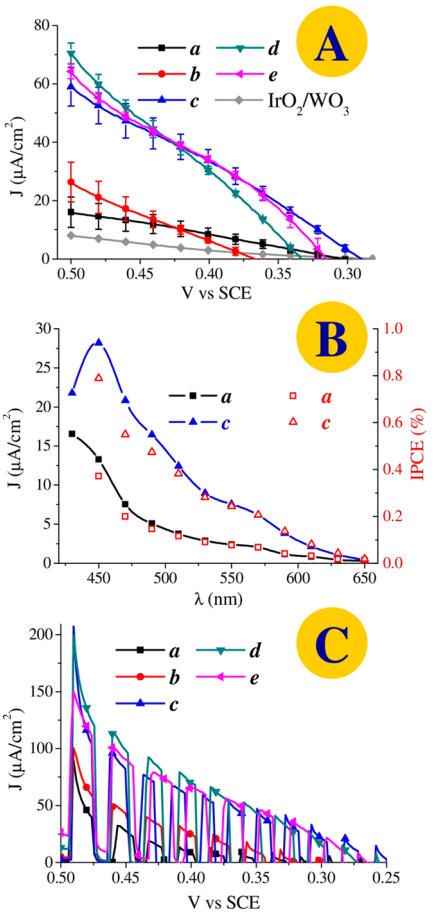

Figure 4. (A) *J*–*V* curves of five different batches of photoelectrodes **1**/WO_3, modified with IrO_2 (***b*–*e***) compared to the unmodified one (***a***). (B) Photocurrent spectra of type ***a*** (black squares) and ***c*** (blue triangles) photoanodes with their relative IPCE spectra (red empty squares and triangles). Data recorded at constant 0.5 V vs SCE in aqueous 0.1 M $NaClO_4$ at pH 3. (C) *J*–*V* curves of the type ***a*–*e*** electrodes under shuttered illumination. AM 1.5 G with 435 nm cutoff in aqueous 0.1 M $NaClO_4$ at pH 3.

the photocurrent transients and their shape, showing a rapidly decreasing photoanodic spike, are indicative of recombination processes in competition with hole transfer to the electrolyte. The charge transfer kinetics, probed at 430 nm (Figure S17), show that, in the presence of codeposited IrO_2, a reduction in the lifetime (0.5 μs) of the photo-oxidized sensitizer on the WO_3 surface is observed, ostensibly due to hole transfer to randomly adjacent IrO_2 NPs. The hole transfer kinetics to IrO_2 thus occurs on the same time scale of electron recapture by $\mathbf{1}^+$, according to an apparent first order rate constant of 0.95×10^6 s^{-1}. Unfortunately the fate of the hole trapped on IrO_2 could not be directly monitored, due to the lack of significant spectroscopic signatures resulting from the oxidation of Ir(IV), as already pointed out by Wasielewski et al.[15] Nevertheless, even for prolonged illumination periods (hundreds of seconds) at constant potential (0.35 V vs SCE), the best **1**/IrO_2/WO_3 assembly (type ***c***) is able to photogenerate a significantly higher anodic charge (up to 5 times) with respect to the unmodified photoelectrodes (type ***a***) (Figure S18).

Experiments carried out with thicker and more optically dense SC6 electrodes (Figure S11), which performed well in the presence of sacrificial agent (Figure S12), did not result in a substantially enhanced photoelectrochemical response in acidic

DOI: 10.1021/jacs.5b01519
J. Am. Chem. Soc. XXXX, XXX, XXX–XXX

$NaClO_4$, when consideration is made for the contribution of the improved bare WO_3 substrate, pointing out the kinetic bottleneck in the hole transfer to codeposited IrO_2 NPs (Figure S19).

In conclusion, we have demonstrated that the modification of WO_3 with simple PBI derivatives, by exploiting aggregation forces, leads to photoanodes where electron injection results in long-lived charge separated states in the heterogeneous phase, where the strong oxidizing power of photogenerated holes can be potentially employed to activate a wide array of catalysts, having E_{ox} < 1.7 V vs SCE, to drive photo-oxidation reactions under visible illumination.

The fact that charge injection on WO_3 is more efficient than on SnO_2, which has a similar conduction band energetics, may underline the role of a higher coupling resulting either from a stronger electrostatic interaction with the negatively charged WO_3 surface at pH 3[23] or by a larger overlap between the d band and the π^* orbitals of **1**.

Clearly, the low conduction band of WO_3, while allowing an efficient quenching of the excited state of PBIs, requires the application of a positive potential to drive the hydrogen evolution reaction at the counter electrode of the PEC. Although this is disadvantageous for a self-standing cell operating without additional bias, it should be recalled that, even when using TiO_2 in sensitized PEC for water splitting, it is often necessary to apply a moderately positive bias, up to 0.3 V vs NHE, to overcome, for both thermodynamic and kinetic reasons, recombination processes. In these cases the sensitized electrode serves only as the photoanodic component of a cell, which will require the coupling to a photocathode, to achieve its independent operation without external potential.

Finally, these porous photoanodes may also constitute a convenient mean to explore and optimize the interaction of the PBI chromophores, immobilized on surfaces, with selected catalytic species, including amorphous metal oxides and molecular species, in order to increase the efficiency of the interfacial charge transfer over competitive carrier recombination, representing, at present, the most serious limitation to molecular level artificial photosynthetic processes.

■ ASSOCIATED CONTENT

Supporting Information

Additional electrochemical, photoelectrochemical, and spectroscopic data; detailed experimental procedures and preparations. This material is available free of charge via the Internet at http://pubs.acs.org.

■ AUTHOR INFORMATION

Corresponding Authors

*cte@unife.it
*g4s@unife.it
*prato@units.it

Notes

The authors declare no competing financial interest.

■ ACKNOWLEDGMENTS

Financial support from FIRB Nanosolar project n.RBAP11C58Y (UNIFE and UNITS) is gratefully acknowledged.

■ REFERENCES

(1) (a) Eisenberg, R.; Nocera, D. *Inorg. Chem.* **2005**, *44*, 6799. (b) Alstrum-Acevedo, J. H.; Brennaman, M. K.; Meyer, T. J. *Inorg. Chem.* **2005**, *33*, 6802. (c) Gust, D.; Moore, T. A.; Moore, A. L. *Acc. Chem. Res.* **2009**, *42*, 1890. (d) Sartorel, A.; Bonchio, M.; Campagna, S.; Scandola, F. *Chem. Soc. Rev.* **2013**, *42*, 2262.

(2) Concepcion, J. J.; House, R. L.; Papanikolas, J. M.; Meyer, T. J. *Proc. Natl. Acad. Sci. U.S.A.* **2012**, *109*, 15560.

(3) (a) Youngblood, W. J.; Anna Lee, S.-H.; Maeda, K.; Mallouk, T. J. *Acc. Chem. Res.* **2009**, *42*, 1966. (b) Zhao, Y.; Swierk, J. R.; Megiatto, J. D., Jr; Sherman, B.; Youngblood, W. J.; Qin, D.; Lentz, L.; Moore, A. L.; Moore, T. A.; Gust, D.; Mallouk, T. E. *Proc. Natl. Acad. Sci. U.S.A.* **2012**, *109*, 15612.

(4) Cowan, A. J.; Durrant, R. J. *Chem. Soc. Rev.* **2013**, *42*, 2281.

(5) Ruttinger, W.; Dismukes, G. C. *Chem. Rev.* **1997**, *97*, 1.

(6) Chen, X.; Mao, S. S. *Chem. Rev.* **2007**, *107*, 2891.

(7) Bignozzi, C. A.; Caramori, S.; Cristino, V.; Argazzi, R.; Meda, L.; Tacca, A. *Chem. Soc. Rev.* **2013**, *42*, 2228.

(8) (a) Sartoretti, C. J.; Alexander, B. D.; Solarska, R.; Rutkowska, I. A.; Augustynski, J. *J. Phys. Chem. B* **2005**, *109*, 13685. (b) Sivula, K.; Le Formal, F.; Graetzel, M. *ChemSusChem* **2011**, *4*, 432.

(9) Abe, R.; Higashi, M.; Domen, K. *J. Am. Chem. Soc.* **2010**, *132*, 11828.

(10) (a) Alibabaei, L.; Brennaman, M. K.; Norris, M. R.; Kalanyan, B.; Song, W.; Losego, M. D.; Concepcion, J. J.; Binstead, R. A.; Parsons, G. N.; Meyer, T. J. *Proc. Natl. Acad. Sci. U.S.A.* **2013**, *110*, 20008. (b) Vannucci, A. K.; Alibabaei, L.; Losego, M. D.; Concepcion, J. J.; Kalanyan, B.; Parsons, G. N.; Meyer, T. J. *Proc. Natl. Acad. Sci. U.S.A.* **2013**, *10*, 20918. (c) Gao, Y.; Ding, X.; Liu, J.; Wang, L.; Lu, Z.; Li, L.; Sun, L. *J. Am. Chem. Soc.* **2013**, *135*, 4219. (d) Gao, Y.; Zhang, L.; Ding, X.; Sun, L. *Phys. Chem. Chem. Phys.* **2014**, *16*, 12008.

(11) Kirner, J. T.; Stracke, J. J.; Gregg, B. A.; Finke, R. G. *ACS Appl. Mater.Interfaces* **2014**, *6*, 13367.

(12) Kanan, M. W.; Nocera, D. G. *Science* **2008**, *321*, 1072.

(13) (a) Schmidt, C. D.; Hirsch, A. *Ideas in Chemistry and Molecular Sciences: Advances in Synthetic Chemistry*; Pignataro, B., Ed.; Wiley WCH: New York, 2010. (b) Li, C.; Wonneberger, H. *Adv. Mater.* **2012**, *24*, 613. (c) Huang, C.; Barlow, S.; Marder, S. R. *J. Org. Chem.* **2011**, *76*, 2386.

(14) (a) Concepcion, J. J.; Jurss, J. W.; Brennaman, M. K.; Hoertz, P. G.; Patrocinio, A. O. T.; Murakami Iha, N. Y.; Templeton, J. L.; Meyer, T. J. *Acc. Chem. Res.* **2009**, *42*, 1954. (b) Kunz, V.; Stepanenko, V.; Wurthner, F. *Chem. Commun.* **2015**, *51*, 290.

(15) Vagnini, M. T.; Smeigh, A. L.; Blakemore, J. D.; Eaton, S. W.; Schley, N. D.; D'Souza, F.; Crabtree, R. H.; Brudvig, G. W.; Co, D. T.; Wasielewski, M. R. *Proc. Natl. Acad. Sci. U.S.A.* **2012**, *109*, 15651.

(16) Weingarten, A. S.; Kazantsev, R. V.; Palmer, L. C.; McClendon, M.; Koltonow, A. R.; SamuelAmanda, P. S.; Kiebala, D. J.; Wasielewski, M. R.; Stupp, S. I. *Nat. Chem.* **2014**, *6*, 964.

(17) (a) Lloret Fillol, J.; Codolà, Z.; Garcia-Bosch, I.; Gomez, L.; Pla, J. J.; Costas, M. *Nat. Chem.* **2011**, *3*, 807. (b) Klepser, B. M.; Bartlett, B. M. *J. Am. Chem. Soc.* **2014**, *136*, 1604.

(18) Gao, F.; Zhao, Y.; Liang, W. *J. Phys. Chem. B* **2011**, *115*, 2609.

(19) Sirimanne, P. M.; Soga, T. *Sol. Energy. Mater. Sol. Cells* **2003**, *80*, 383.

(20) The injection rate constant measured by TCSPC has to be considered as an average lower limit to the rate constant, given that processes faster than 300 ps fall within the excitation profile of the pulsed led source and cannot be appropriately deconvolved.

(21) Hara, M.; Warakasa, C. C.; Lean, J. T.; Lewis, B. A.; Mallouk, T. E. *J. Phys. Chem.B* **2000**, *104*, 5275.

(22) Youngblood, W. J.; Lee, S.-H. A.; Kobayashi, Y.; Hernandez-Pagan, E. A.; Hoertz, P. G.; Moore, T. A.; Moore, A. L.; Gust, D.; Mallouk, T. E. *J. Am. Chem. Soc.* **2009**, *131*, 926.

(23) Kim, J.; Lee, C. W.; Choi, W. *Environ. Sci. Technol.* **2010**, *44*, 6849.

DOI: 10.1021/jacs.5b01519
J. Am. Chem. Soc. XXXX, XXX, XXX−XXX